Nuclear Materials and Energy 39 (2024) 101650

Contents lists available at ScienceDirect

Nuclear Materials and Energy

journal homepage: www.elsevier.com/locate/nme

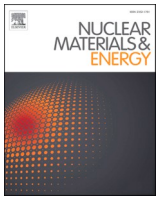

Reaction kinetics of Li_4SiO_4 and $Li_4Ti_5O_{12}$ in biphasic breeder ceramics after lithium burn-up

Julia Leys [*], Christina Odenwald [1], Regina Knitter

Karlsruhe Institute of Technology (KIT), Institute for Applied Materials (IAM), 70621 Karlsruhe, Germany

ARTICLE INFO

Keywords:
Biphasic ceramic breeder
Lithium burn-up
Reaction kinetics
Lithium silicates
Lithium titanates

ABSTRACT

Advanced ceramic breeder (ACB) pebbles consisting of the two phases Li_4SiO_4 and Li_2TiO_3 serve as the EU reference tritium breeding material. In the present study, the phase stability with regard to a lithium-burn-up is investigated. The loss of lithium due to its transmutation will lead to a compositional change of the breeder material. Li_4SiO_4 and Li_2TiO_3 will partly be transformed to the lithium-poorer phases Li_2SiO_3 and $Li_4Ti_5O_{12}$, respectively. However, from the phase diagram it is anticipated that only Li_2SiO_3 will occur as a third phase after a lithium burn-up as the generated $Li_4Ti_5O_{12}$ is expected to further react with Li_4SiO_4 to form again Li_2TiO_3 and more Li_2SiO_3. Therefore, the reaction between Li_4SiO_4 and $Li_4Ti_5O_{12}$ and its temperature dependence were investigated in detail and its reaction kinetics were determined. It was found that this diffusion-controlled reaction with an activation energy of 75 kJ/mol (0.78 eV) will slow down at low irradiation temperatures and may not take place at very low temperatures.

1. Introduction

Advanced ceramic breeder (ACB) pebbles consisting of lithium orthosilicate (Li_4SiO_4) with additions of lithium metatitanate (Li_2TiO_3) were qualified in the past as favourable tritium breeder material and exhibit the EU reference tritium breeding material [1]. While Li_4SiO_4 provides a high lithium density, Li_2TiO_3 improves the thermal and mechanical stabilities. Additions of up to 35 mol% Li_2TiO_3 are considered for its application in ITER and DEMO [2].

In a nuclear fusion power plant, lithium from the breeder blanket is partially consumed due to the tritium breeding. Hence, a continuous change in the chemical composition of the initial biphasic breeder material occurs, finally leading to a triphasic composition of Li_4SiO_4, Li_2TiO_3, and lithium metasilicate (Li_2SiO_3) (see eq. (1)).

$$a\mathbf{Li_4SiO_4} + b\mathbf{Li_2TiO_3} \rightarrow a(1-2x) - b\left(\frac{1}{15}x\right)\mathbf{Li_4SiO_4} + a(2x) + 3b\left(\frac{1}{15}x\right)\mathbf{Li_2SiO_3} + b\mathbf{Li_2TiO_3} + a(2x) + b\left(\frac{2}{5}x\right)\left(\mathbf{He} + \frac{1}{2}\mathbf{T_2O}\right) \quad (1)$$

with a and b = molar fractions and x = fractions of burn-up.

Considering a ternary phase diagram [3] only Li_2SiO_3 should occur as a third phase after the lithium burn-up. This is shown in Fig. 1, where the arrow shows the compositional change up to a lithium burn-up of 50 % for a starting ACB composition of 70 mol% Li_4SiO_4 and 30 mol% Li_2TiO_3. After a burn-up of even 50 % of the initial lithium, the material would lie in the stability field of the three phases Li_4SiO_4, Li_2TiO_3 and Li_2SiO_3.

In contrast, the reactions of the single-phase materials correspond to the equations (2) and (3). Here, the tritium breeding going along with a lithium loss in Li_4SiO_4 leads to the partial formation of the phase Li_2SiO_3 [4]. The situation for Li_2TiO_3 is different as its structure is more flexible with regard to the lithium content. Li_2TiO_3 has an extended stability range and can be non-stoichiometric: below 1050 °C monoclinic lithium metatitanate solid solutions are stable in the range of 49–53 mol% Li_2O [5,6]. For lower Li_2O contents, lithium titanate ($Li_4Ti_5O_{12}$) is partially formed. The experimental proof of the formation of $Li_4Ti_5O_{12}$ from Li_2TiO_3 during neutron irradiation was recently published [7].

$$a\mathbf{Li_4SiO_4} \rightarrow a(1-2x)\mathbf{Li_4SiO_4} + a(2x)\mathbf{Li_2SiO_3} + a(4x)\left(\mathbf{He} + \frac{1}{2}\mathbf{T_2O}\right) \quad (2)$$

$$b\mathbf{Li_2TiO_3} \rightarrow b\left(1-\frac{1}{3}x\right)\mathbf{Li_2TiO_3} + b\left(\frac{1}{15}x\right)\mathbf{Li_4Ti_5O_{12}} + b\left(\frac{2}{5}x\right)\left(\mathbf{He} + \frac{1}{2}\mathbf{T_2O}\right) \quad (3)$$

* Corresponding author.
E-mail address: julia.leys@kit.edu (J. Leys).
[1] Current affiliation: Saarland University, Inorganic Solid-State Chemistry, 66123 Saarbrücken, Germany.

https://doi.org/10.1016/j.nme.2024.101650
Received 4 March 2024; Received in revised form 3 April 2024; Accepted 4 April 2024
Available online 4 April 2024

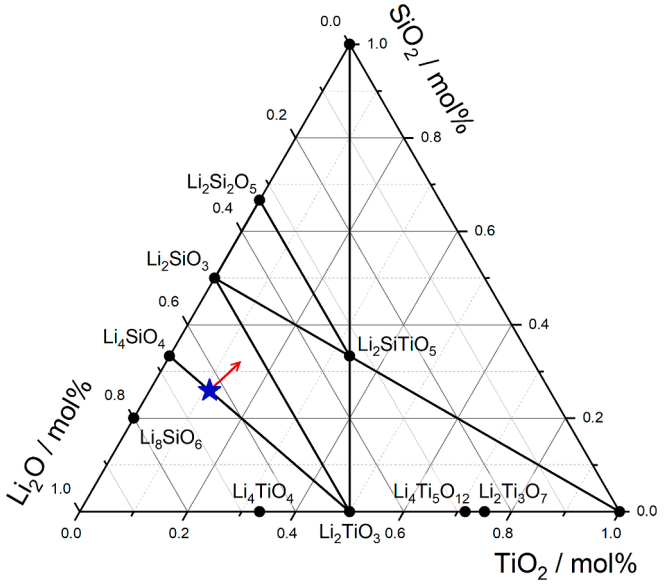

Fig. 1. Ternary phase diagram of Li_2O-SiO_2-TiO_2 after Hanoar et al. [3]. The blue star represents the ACB composition of 70 mol% Li_4SiO_4 and 30 mol% Li_2TiO_3. The red arrow shows the path for a lithium burn-up up to 50 %. (For interpretation of the references to colour in this figure legend, the reader is referred to the web version of this article.)

with a and b = molar fractions and x = fractions of burn-up.

In the case of a coexistence of Li_4SiO_4 and $Li_4Ti_5O_{12}$, these phases further react to Li_2TiO_3 and Li_2SiO_3 (see eq. (4)). This underlines the lithium burn-up reaction of Li_4SiO_4 and Li_2TiO_3 described in equation (1) leading to only one additional phase after the lithium burn-up.

$$3\,Li_4SiO_4 + Li_4Ti_5O_{12} \rightarrow 5\,Li_2TiO_3 + 3\,Li_2SiO_3 \quad (4)$$

As the two phases within the ACB pebbles are not finely dispersed as in a powder, the potential formation of $Li_4Ti_5O_{12}$ should be considered. And therefore, it is important to understand at which conditions the reaction takes place, especially, as the ACB pebbles experience different temperatures in the blanket within a broad range of about 400 to >900 °C [8]. A change in composition and in particular a temporary existence of $Li_4Ti_5O_{12}$ could lead to a change in the material properties and might be an important issue to be considered for the behaviour of the blanket.

First experiments on this topic were accomplished by Xiang et al. [9]. They prepared Li_4SiO_4, Li_2TiO_3 and Li_4SiO_4–Li_2TiO_3 powders with a simulated lithium burn-up and analysed them with X–ray diffraction (XRD) at room temperature and simultaneous thermogravimetry and differential scanning calorimetry (TG-DSC) up to 800 °C. Their studies confirmed that $Li_4Ti_5O_{12}$ could only be detected in the Li_2TiO_3 sample with lithium deficiency. The Li_4SiO_4–Li_2TiO_3 sample did not show any occurrence of $Li_4Ti_5O_{12}$ even at the highest simulated burn-up of 20 %. The TG/DSC studies suggested that the reaction between Li_4SiO_4 and $Li_4Ti_5O_{12}$ takes place at about 655 °C [8].

In the present study, the described results are extended and new experiments are performed. The kinetics of the reaction between Li_4SiO_4 and $Li_4Ti_5O_{12}$ were investigated in detail. Therefore, the reactions of powder mixtures and contacting pellets of Li_4SiO_4 and $Li_4Ti_5O_{12}$ were evaluated for different dwell times and at different temperatures. From the results, the kinetic constants and the activation energy of the reaction were derived.

2. Material and methods

2.1. Powder samples

The following starting powders were used: Tetraethoxysilane (TEOS, > 99 %) and titanium tetra-isopropoxide (TTIP, > 98 %) were purchased from *Merck*, lithium titanium oxide ($Li_4Ti_5O_{12}$, > 95 %) was obtained from *Süd-Chemie* and nitric acid (HNO_3, 65 %) was purchased from *VWR*. Lithium hydroxide monohydrate ($LiOH{\cdot}H_2O$, 99.995 %) and lithium orthosilicate (Li_4SiO_4, 99.9 %) were purchased from *Alfa Aesar*. These chemicals were used as received.

Li_4SiO_4 was synthesised via a sol–gel route similar to Hanoar et al. [3] as no material with sufficient purity could commercially be obtained. Therefore, TEOS was dissolved in absolute ethanol (c = 0.14 mol/l) and stirred for about 20 min at room temperature. Then, an ethanolic solution of nitric acid (c = 0.07 mol/l) was added. After stirring the solution for about 5 h, $LiOH{\cdot}H_2O$ in the respective molar ratio was added. After vigorous stirring for almost 24 h, the solvent of the turbid solution was removed under reduced pressure (40 °C, 175 mbar) and a white, finely pulverised solid was obtained. This powder was then dried in vacuum (180 °C, 20 mbar, 2 h). As the as-received powder from the sol–gel synthesis is amorphous, the powder was calcined (2 h at 600 °C, 5 K/min) and sintered (9 h at 900 °C, 5 K/min) in a covered platinum crucible.

2.2. Pellet samples

Pellets for the contact tests were prepared in the following way. In order to avoid a strong shrinkage of the pellets and pore formation during the subsequent temperature treatment, calcined powder was used (2 h at 600 °C, 5 K/min). The calcined material was pressed into pellets ($Ø_{pellet}$ = 13 mm, h_{pellet} = 13.5 mm, F_{press} = 15 kN) and sintered on a platinum plate at 900 °C for 9 h (heating rate = 5 K/min). Commercially available Li_4SiO_4 was placed next to the sample in the furnace as sacrificial material during the calcination and sintering steps to avoid a lithium loss during the temperature treatment.

For the preparation of the $Li_4Ti_5O_{12}$ pellets, a press granulate ($Ø_{pellet}$ = 13 mm, F_{press} = 25 kN) was produced from the solid material, which was then pressed into pellets ($Ø_{pellet}$ = 13 mm, h_{pellet} = 13.5 mm, F_{press} = 15 kN). The pellets were sintered on a platinum plate at 900 °C for 8 h (heating rate = 5 K/min).

The surfaces of all pellets were ground smooth after the temperature treatment to enhance the contact within the contact tests.

2.3. Contact tests of Li_4SiO_4 and $Li_4Ti_5O_{12}$

In order to investigate the reaction rate between Li_4SiO_4 and $Li_4Ti_5O_{12}$, pellets of the two pure phases were brought into contact with each other and treated in a furnace at 700, 800, or 900 °C for 10–480 h. The phase composition of the pellets was analysed by XRD before and after each contact test. The $Li_4Ti_5O_{12}$ pellet was placed at the bottom of a platinum crucible and the Li_4SiO_4 pellet was positioned centrically on top. To ensure a good contact, another smaller platinum crucible filled with alumina weights (approx. 14 g) was placed on top of the Li_4SiO_4 pellet. The outer crucible was covered with a platinum lid and the pellets were heated in air with 5 K/min to the planned annealing temperature. After the chosen reaction time, the pellets were cut, embedded in an epoxy resin under vacuum and the samples were ground and polished. SEM images of the cross-sectional areas were taken. In Fig. 2 the set-up of the contact tests and the further pellet procedure is schematically shown.

In addition, some tests were performed with powders. Therefore, Li_4SiO_4 powder was mixed with $Li_4Ti_5O_{12}$ powder in a mole ratio of 3:1. High temperature XRD (HT–XRD) and TG-DSC were used to investigate the reaction between the two phases in situ. Furthermore, the mixture was heat treated at 550 °C for 48 h and at 500, 450, and 400 °C for 240 h

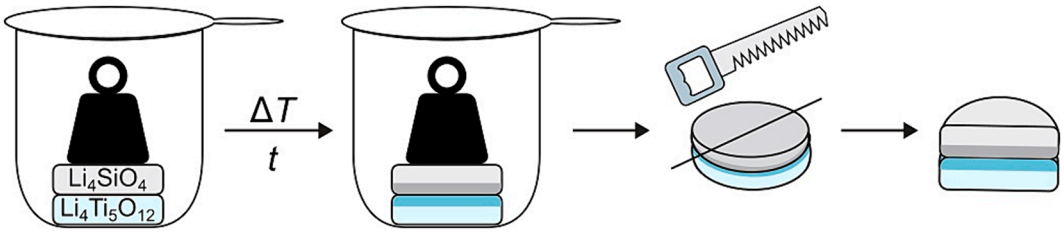

Fig. 2. Schematic of the set-up of the pellet contact tests and the preparation of the pellets for SEM analyses. Both pellets are white, colours are only used to improve visualisation.

in a furnace and afterwards analysed by XRD.

2.4. Analytical methods

The synthesised powders as well as powders after TG-DSC measurements were analysed with regard to their phase composition using powder XRD applying a *D2 PHASER* diffractometer (*Bruker AXS*) with Cu-Kα in air (10–85°, 0.02°/step, 1 s/step, 15 rpm). Furthermore, the phase compositions of the pellets before and after the contact tests were evaluated using XRD (10–80°, 0.02°/step, 0.04 s/step, no rotation).

For a powder mixture of Li_4SiO_4:$Li_4Ti_5O_{12}$ (3:1 mol%) HT–XRD patterns were recorded. Measurements were performed using a *D8 ADVANCE* diffractometer (*Bruker AXS*) with a heating chamber (*Anton Paar HTK 1200 N*) using Cu–Kα radiation in air (15–100°, 0.02°/step, 0.6 s/step, no rotation). 20 temperature steps were performed from room temperature up to 900 °C.

To verify the phase compositions, the following reflection positions were used as reference data: Li_4SiO_4 (ICSD-25759, [10]), Li_2SiO_3 (ICSD-16626, [11]), Li_2TiO_3 (ICSD-15150, [12]), and $Li_4Ti_5O_{12}$ (ICSD-185587, [13]).

The cross sections of the pellets were analysed by SEM (*Zeiss SUPRA 55* microscope with angular selective backscattered electrons (AsB) detector). The embedded samples were sputtered with a thin Au-Pd layer. All SEM images were recorded with an acceleration voltage of 10 kV and a working distance of about 5 mm. The thicknesses of the reaction layers of the $Li_4Ti_5O_{12}$ pellets were measured with *ImageJ* (v. 1.52a) from the SEM images. To measure the layer thickness in the micrograph, a magnification of 300 was used. For each sample, 30 values were recorded and averaged.

For TG–DSC analyses a *Netzsch STA 449 F3* device was used. Measurements in platinum alloy (PtRh20) crucibles were performed from room temperature to 1000 °C in synthetic air within two subsequent cycles. A heating/cooling rate of 10 K/min was adjusted and a correction curve was applied to reduce buoyancy effects. The measurements were performed three times to ensure repeatability.

3. Results and discussion

In order to determine whether a reaction between Li_4SiO_4 and $Li_4Ti_5O_{12}$ takes place and in which temperature range, the two substances were mixed as powders and the temperature-dependent change of the phase composition was monitored by in situ HT-XRD. For the powder mixture a ratio of Li_4SiO_4:$Li_4Ti_5O_{12}$ = 3:1 mol% was chosen to enable a complete conversion. Fig. 3 displays diffraction patterns at selected temperatures and reference reflection positions for the different phases. It has to be considered that the reflection peaks shift to lower angles at elevated temperatures. At room temperature, only the reflections of Li_4SiO_4 and $Li_4Ti_5O_{12}$ are present. A decrease of Li_4SiO_4 combined with the formation of Li_2SiO_3 is observed from approximately 570 °C. The decrease of $Li_4Ti_5O_{12}$ and the formation of Li_2TiO_3 is observable from 590 °C. As a zoom in to the respective 2 theta region is necessary to see the first effects, they can hardly be observed in Fig. 3 at the mentioned temperatures. However, in the resolution of the displayed patterns the first peaks of Li_2SiO_3 and Li_2TiO_3 are visible in the next higher temperature step at 590 and 610 °C, respectively. At 800 °C no reflections of Li_4SiO_4 can be observed any more. However, the reflections of $Li_4Ti_5O_{12}$ only disappear at 900 °C with the given heating conditions.

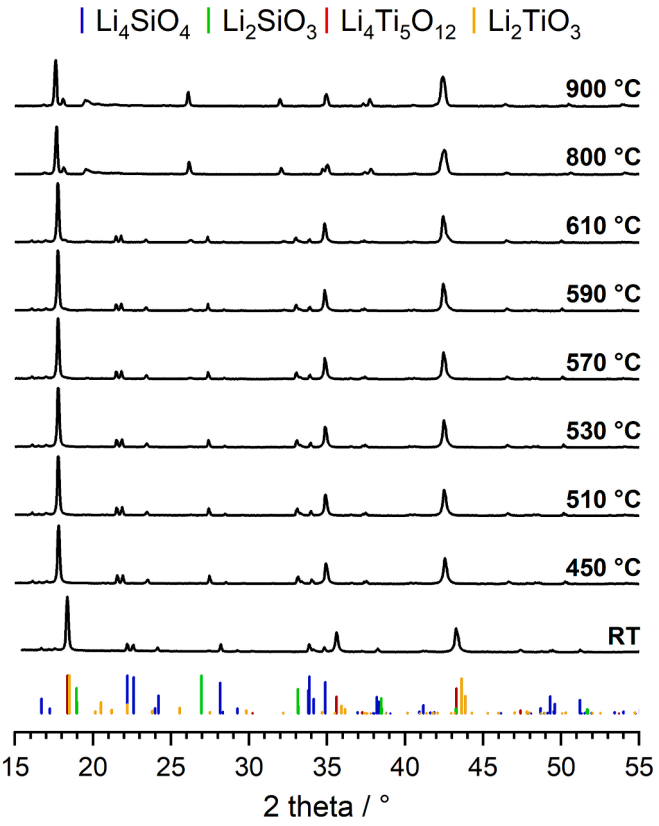

Fig. 3. Selected HT-XRD patterns of a 3:1 mol% Li_4SiO_4:$Li_4Ti_5O_{12}$ powder mixture from room temperature (RT) to 900 °C. Reference reflections show the two phases Li_4SiO_4 (blue) and $Li_4Ti_5O_{12}$ (red). With increasing temperature, Li_2SiO_3 (green) and Li_2TiO_3 (orange) are formed (cf. eq. (4)). (For interpretation of the references to colour in this figure legend, the reader is referred to the web version of this article.)

The same powder mixture as the one used for the HT-XRD experiment was tempered at 550 °C for 48 h and at 500, 450, and 400 °C for 240 h to investigate if the reaction takes place at these temperatures when it is annealed for a longer time. The XRD patterns of the annealed powder mixtures are shown in Fig. 4. For all annealing temperatures, the reflections of Li_2SiO_3 can be detected besides Li_4SiO_4 and $Li_4Ti_5O_{12}$. Again, the intensity is too low to see the peaks in the resolution of Fig. 4. The reflection peaks of Li_2TiO_3 are also obvious in the diffraction patterns performed after 550, 500 and 450 °C, but can hardly be seen in the pattern after heat treatment at 400 °C for 240 h. However, as the reflection peaks of Li_2SiO_3 are present even only with low intensities, it can be assumed that the intensity of the Li_2TiO_3 is too low to be visible.

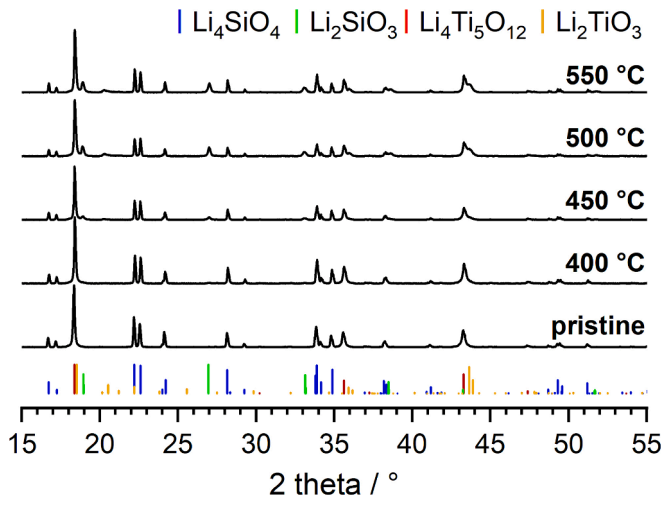

Fig. 4. XRD patterns after the annealing of a 3:1 mol% Li_4SiO_4:$Li_4Ti_5O_{12}$ powder mixture at different temperatures for 240 h (550 °C only for 48 h). Reference reflections show the two phases Li_4SiO_4 (blue) and $Li_4Ti_5O_{12}$ (red). With increasing temperature, Li_2SiO_3 (green) and Li_2TiO_3 (orange) are formed (cf. eq. (4)). (For interpretation of the references to colour in this figure legend, the reader is referred to the web version of this article.)

Therefore, it can be concluded that the reaction between Li_4SiO_4 and $Li_4Ti_5O_{12}$ also takes place at lower temperatures such as ≥400 °C.

The phase changes of a 3:1 mol% powder mixture of Li_4SiO_4 and $Li_4Ti_5O_{12}$ were investigated by thermal analysis, where the powder mixture was heated up to 1000 °C for two times. The DSC curves from 200 to 1000 °C are displayed in Fig. 5, here the curves from thermal gravimetry were left out for better clarity and because no relevant changes were observed.

The most characteristic feature with endothermic peaks in both cycles is the triple phase transition in Li_4SiO_4 between 600 and 725 °C (indicated as green circles in Fig. 5) [14,15]. These peaks are less pronounced in the second cycle, because more Li_4SiO_4 is already consumed for the reaction with $Li_4Ti_5O_{12}$. Yet the appearance also indicate that the reaction is incomplete even in the second cycles. Both cycles also show a prominent endothermic peak at approximately 950 °C, which exhibits a shoulder to higher temperatures in the first cycle. This peak refers to the phase transition of the monoclinic β–Li_2TiO_3 to the cubic γ–Li_2TiO_3 (indicated as a black diamond in Fig. 5) that is lowered down from 1155 °C to 930 °C in the presence of $Li_4Ti_5O_{12}$ [16].

Additional peaks can be observed in the first cycle. Two relatively broad, endothermic peaks at about 260 °C and 795 °C cannot be explained. Considering the results from XRD, the first peak below 300 °C cannot be related to the reaction between Li_4SiO_4 and $Li_4Ti_5O_{12}$. Also, for the peak at about 800 °C no possible phase transition can be found for the relevant compositions, neither in the Li_2O-TiO_2 nor in the Li_2O-SiO_2 phase diagram [4,6,16]. Another broad, asymmetric and more intense peak at about 490 °C is presumed to be associated with the reaction between Li_4SiO_4 and $Li_4Ti_5O_{12}$ (indicated as a red star in Fig. 5). This reaction was observed to already take place at 400 °C in the annealed powder mixtures, but is here shifted to higher temperatures due to the relatively high heating rate of 10 K/min. It seems implausible that the two further peaks of very low intensity at approximately 370 °C and 390 °C are also related to the phase reaction, yet it cannot be completely ruled out that the reaction occurs at different points within the sample at different temperatures due to a certain inhomogeneity of the sample. However, if the reaction energy is intense enough to be observed for partial reactions, the reaction should also be observed in the second cycle, where $Li_4Ti_5O_{12}$ is still present. In any case, a reaction temperature of 655 °C observed by Xiang et al. also with a heating rate of 10 K/min but under argon cannot be confirmed here [9].

XRD patterns recorded after the thermal analysis showed the four phases Li_2TiO_3, Li_2SiO_3, $Li_4Ti_5O_{12}$ and Li_4SiO_4. Although not all Li_4SiO_4 and $Li_4Ti_5O_{12}$ were consumed, a significant reduction of the two initial phases can be observed. A comparison of the XRD patterns before and after the thermal analysis is shown in Fig. A1 in the supplementary information.

Contact tests using pellets were performed to examine the kinetics of the reaction between Li_4SiO_4 and $Li_4Ti_5O_{12}$. Before and after each contact test, XRD patterns of the contact surfaces of the pellets were

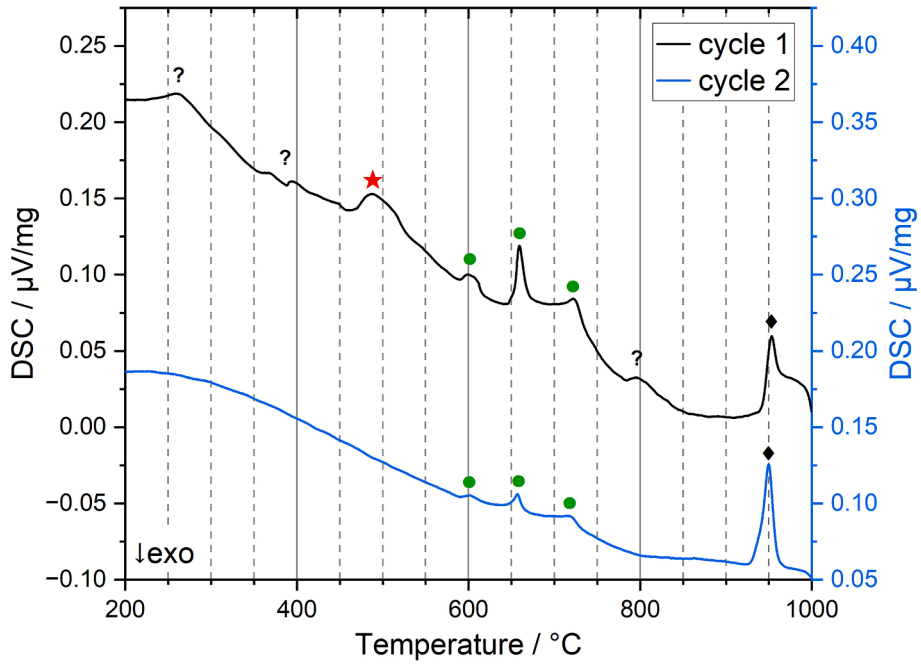

Fig. 5. DSC curves of a 3:1 mol% Li_4SiO_4:$Li_4Ti_5O_{12}$ powder mixture for two cycles (upper line, black: 1st cycle, lower line, blue: 2nd cycle). The peaks are indicated as the following: green circles = phase transitions of Li_4SiO_4, black diamond = phase transition of Li_2TiO_3 (β → γ), and red star = the peak presumed to represent the reaction between Li_4SiO_4 and $Li_4Ti_5O_{12}$. (For interpretation of the references to colour in this figure legend, the reader is referred to the web version of this article.)

recorded. Fig. 6 shows diffraction patterns of the Li_4SiO_4 pellets treated at 800 °C with different dwell times. Before the contact experiment (i.e., 0 h in Fig. 6) the pellets consist of pure Li_4SiO_4. With an increasing dwell time, an increased conversion into Li_2SiO_3 is observed. After 160 h, only small amounts of Li_4SiO_4 are visible in the diffraction pattern. XRD patterns of the Li_4SiO_4 from the contact tests at 700 and 900 °C are shown in figures A2 and A3, respectively, in the supplementary information.

The XRD patterns of the $Li_4Ti_5O_{12}$ pellets show a similar progression. The XRD patterns of the $Li_4Ti_5O_{12}$ from the contact tests at 700, 800 and 900 °C are given in figures A4, A5 and A6, respectively, in the supplementary information. With an increasing dwell time the intensity of the reflections of $Li_4Ti_5O_{12}$ decreases and that of the Li_2TiO_3 reflections increases for all temperatures. However and as expected, the phase transformations take place faster with increasing temperature. The results confirm that at temperatures between 700 and 900 °C diffusion of lithium from the Li_4SiO_4 pellet to the $Li_4Ti_5O_{12}$ pellet occurs, accompanied by reaction and phase transformations.

To investigate the kinetics of these processes more detailed, SEM analyses of the cross sections of the pellets after the reaction were performed. Fig. 7 gives an example of the cross-sectional area of the pellets after the contact experiment at 900 °C and 80 h. By using an AsB detector, material contrasts are visualised particularly clearly.

The Li_4SiO_4 pellet has a higher porosity than the $Li_4Ti_5O_{12}$ pellet, which was already the case before the reaction, and shows the reaction layer in the lower, slightly lighter part where Li_2SiO_3 is formed. In the case of the $Li_4Ti_5O_{12}$ pellet, the upper, darker reaction layer with Li_2TiO_3 shows a better contrast and higher density, why the reaction front is more clearly defined. Due to its low mass, lithium produces only a small number of backscattered electrons, so that here lithium-richer areas appear dark while heavy elements lead to a stronger backscatter and thus lighter areas. Therefore, the formation of the darker reaction layer in the $Li_4Ti_5O_{12}$ pellet agrees with an increase of lithium due to the formation of Li_2TiO_3 in this area. In Fig. 8 the SEM images of the $Li_4Ti_5O_{12}$ pellets from the experiments at 900 °C and different dwell times are displayed. With increasing reaction time, an increase of the layer thickness is observed.

The mean layer thickness (i.e. depth of reaction) d of the $Li_4Ti_5O_{12}$ pellets at 700, 800 and 900 °C were measured (see Table 1) and plotted against the dwell time (see Fig. 9 (left)). As mentioned before, the $Li_4Ti_5O_{12}$ pellets were used for the determination of the layer thickness

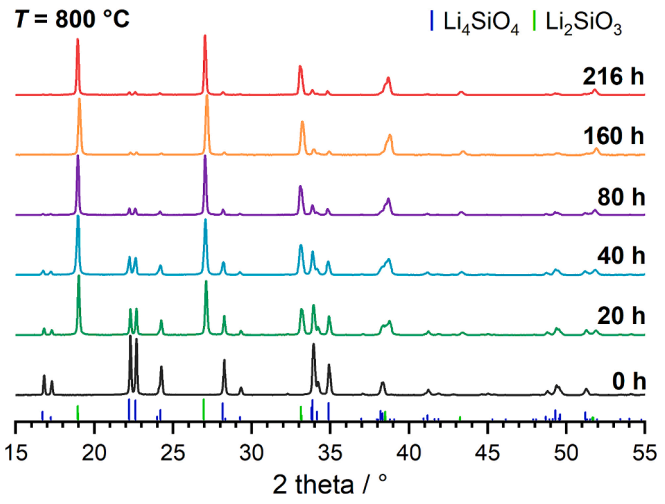

Fig. 6. XRD patterns of the contact surfaces of Li_4SiO_4 pellets before (i.e. 0 h) and after the contact experiments with different dwell times and reference reflection positions of Li_4SiO_4 and Li_2SiO_3 in blue and green, respectively. (For interpretation of the references to colour in this figure legend, the reader is referred to the web version of this article.)

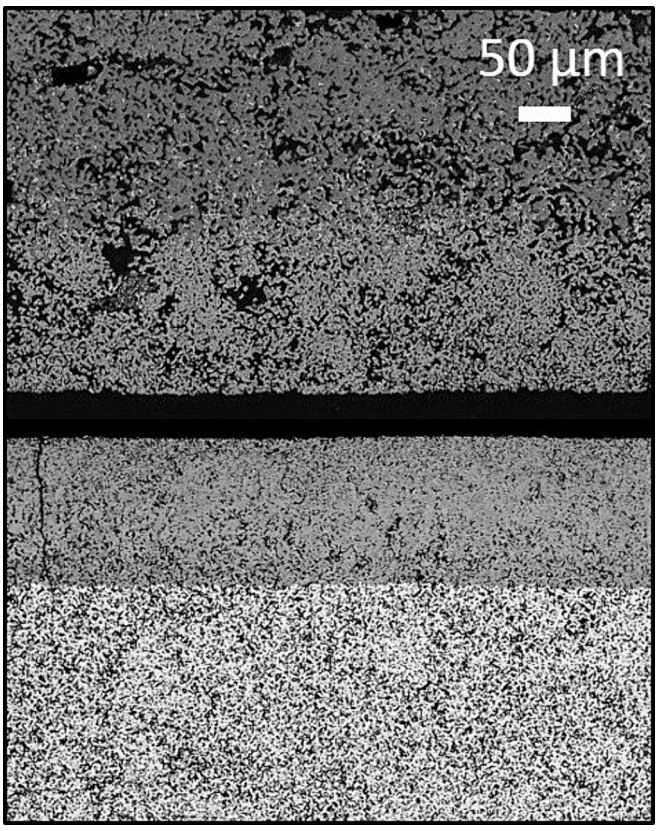

Fig. 7. Cross-section images using an AsB detector of Li_4SiO_4 (top) and $Li_4Ti_5O_{12}$ pellets (bottom) annealed at 900 °C for 80 h.

due to its higher density and a more clearly appearing reaction front. Still, the Li_4SiO_4 pellets also show a corresponding, less clearly pronounced growth of the reaction layer.

The growth of the layer thickness in the considered temperature and time range is reduced with increasing reaction time and can be expressed by a square root function (eq. (5)), indicating a diffusion-controlled growth.

$$d = k \cdot t^{1/2} \tag{5}$$

with d = average depth of reaction in the $Li_4Ti_5O_{12}$ pellet, k = growth rate constant and t = reaction time.

Fig. 9 (right) shows the linearised representation of the graphs in Fig. 9 (left). From the slope of the linear fits the corresponding rate constants k were determined for the three temperatures (see Table 1).

The temperature dependence of the rate constant is given by the Arrhenius diagram (see Fig. 10). The activation energy can be derived from the slope of the linear fit in the Arrhenius plot (see eq. (6)).

$$ln(k) = ln(A) - \frac{E_a}{R} \cdot \frac{1}{T} \tag{6}$$

with k = growth rate constant, A = pre-exponential factor, E_a = activation energy, R = universal gas constant, T = temperature.

The slope of the fit function is $-9.0(6) \cdot 10^3$ K and for the intercept a value of $-7.5(6)$ m·s$^{-1/2}$ is obtained. From these values, an Arrhenius pre-exponential factor of $5.4 \cdot 10^4$ and an activation energy of 75 kJ/mol are determined.

The derived values were used to estimate the thickness of the reaction layer at 400 °C. As an example, the time of 240 h was considered as it was used for the heat treatment of the powder mixture. After 240 h, the thickness of the reaction layer between Li_4SiO_4 and $Li_4Ti_5O_{12}$ can be estimated to be about 1 µm.

Due to a homogenous lithium burn-up under operation, $Li_4Ti_5O_{12}$

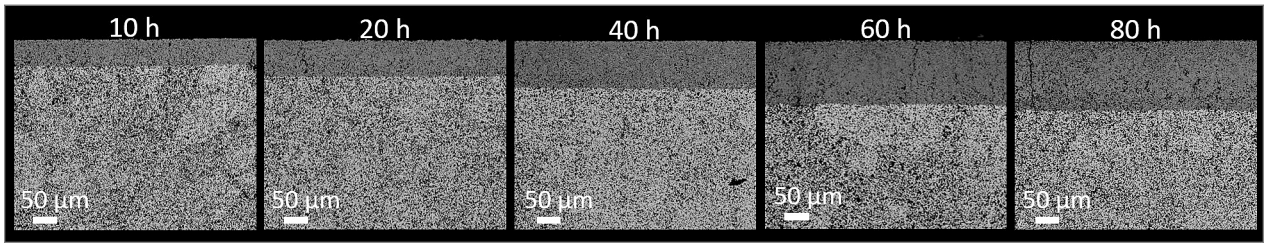

Fig. 8. SEM AsB detector images of $Li_4Ti_5O_{12}$ pellets after the reaction at 900 °C for different dwell times.

Table 1
Temperatures (T) and dwell times (t) of the performed pellet contact tests, the averaged measured reaction layer thicknesses (d) measured from the $Li_4Ti_5O_{12}$ pellets, and the determined growth rate constants (k).

T / °C	t / h	d / µm	k / µm·h$^{-1/2}$	$k \cdot 10^{-8}$ / m·s$^{-1/2}$
700	60	22(1)	3.2(1)	5.3
	120	36(2)		
	180	37(2)		
	240	51(2)		
	480	75(2)		
800	20	25(2)	6.9(3)	11.5
	40	46(3)		
	80	62(3)		
	160	80(4)		
	216	108(3)		
900	10	53(2)	15.5(3)	25.9
	20	71(2)		
	40	95(1)		
	60	126(2)		
	80	138(2)		

will initially be formed as small inclusions within the Li_2TiO_3 grains. There will always be sufficient Li_4SiO_4 for the reaction as it is in any case the main phase of the ACB material, yet at blanket positions with very low temperatures (i.e. $T < 400$ °C), the diffusion-controlled reaction may be too slow to transform all generated $Li_4Ti_5O_{12}$.

4. Conclusions

It is well known that a lithium burn-up will result in the third phase Li_2SiO_3 for the biphasic ACB material consisting of Li_4SiO_4 and Li_2TiO_3. Within this study, the reaction of Li_4SiO_4 with $Li_4Ti_5O_{12}$ was studied in order to be able to make predictions of the existence of $Li_4Ti_5O_{12}$ as a potential fourth phase in the blanket after the lithium burn-up.

Using HT-XRD, the start of the reaction could be observed at about 570 °C in the small sample volume. Further experiments of annealed powder mixtures show the beginning of the reaction already at 400 °C after 240 h. Thermal analysis suggests the main reaction at about 490 °C.

The kinetics of the reaction were determined from contact tests with Li_4SiO_4 and $Li_4Ti_5O_{12}$ pellets. Both pellets show reaction layers of Li_2SiO_3 or Li_2TiO_3, respectively, at their contact surfaces. The rate constants were determined from experiments at temperatures of 700, 800 and 900 °C. From an Arrhenius plot an activation energy of 75 kJ/mol (0.78 eV) was derived for the reaction of Li_4SiO_4 with $Li_4Ti_5O_{12}$. It could be confirmed that the reaction takes already place at 400 °C, but the reaction rate is very low.

Under operation a significant volume of the ACB pebbles will be in the temperature range of 400 to 500 °C with respect to the current DEMO HCPB blanket design [8]. Due to the homogenous lithium burn-up, $Li_4Ti_5O_{12}$ will initially be formed as small inclusions within the Li_2TiO_3 grains. There will always be sufficient Li_4SiO_4 for the reaction as it is in any case the main phase of the ACB material. Yet, at blanket

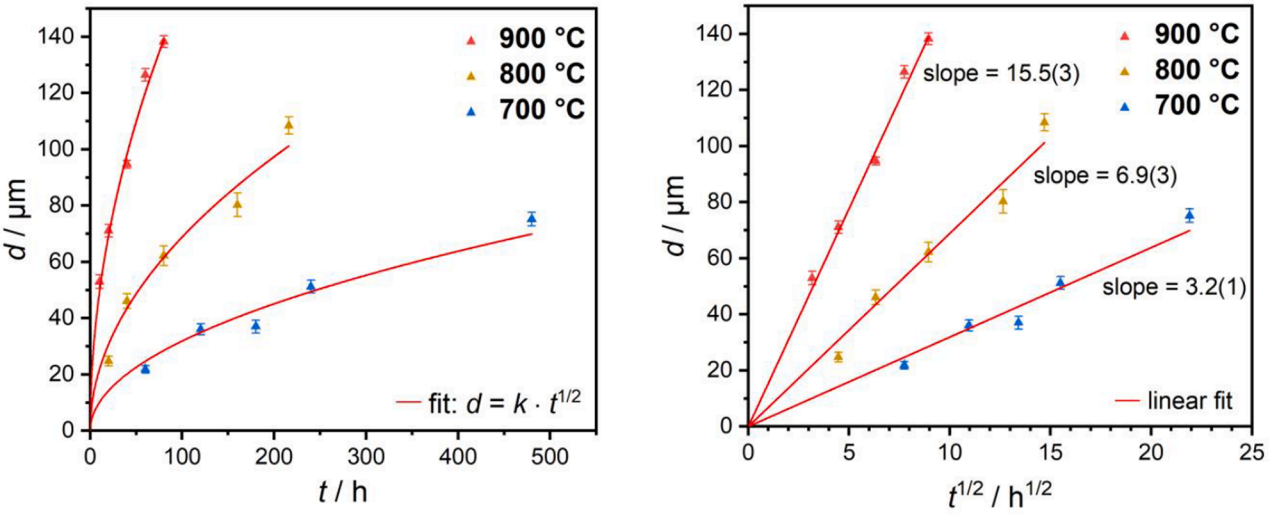

Fig. 9. Layer thickness in $Li_4Ti_5O_{12}$ pellet vs. dwell time at different temperatures and square root fits (left) and vs. square root of dwell time at different temperatures and linear fits (right).

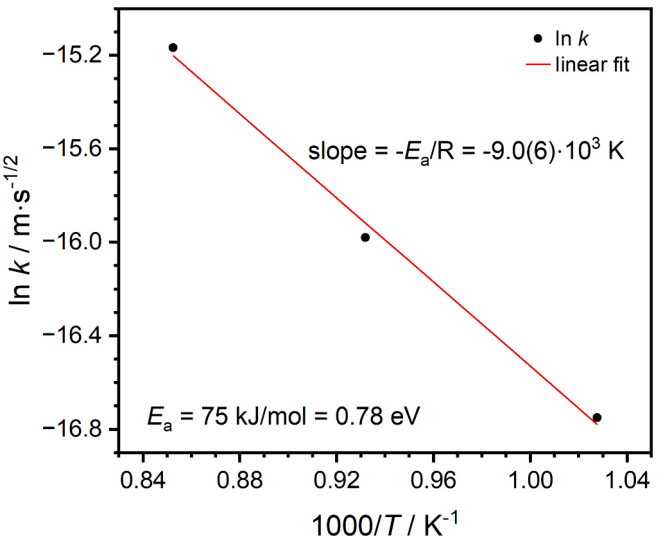

Fig. 10. Arrhenius plot of the growth rate constants determined from the layer thicknesses at the respective temperatures. The activation energy is derived from the slope of the linear fit.

positions with very low temperatures ($T \leq 400$ °C), the diffusion-controlled reaction may be too slow to transform all generated $Li_4Ti_5O_{12}$ immediately, so that the existence of $Li_4Ti_5O_{12}$ on an impurity level cannot be excluded.

CRediT authorship contribution statement

Julia Leys: Writing – original draft, Visualization, Validation, Project administration, Methodology, Investigation, Data curation, Conceptualization. **Christina Odenwald:** Writing – review & editing, Visualization, Validation, Methodology, Investigation, Conceptualization. **Regina Knitter:** Writing – review & editing, Supervision, Resources, Funding acquisition, Conceptualization.

Declaration of competing interest

The authors declare that they have no known competing financial interests or personal relationships that could have appeared to influence the work reported in this paper.

Data availability

Data will be made available on request.

Acknowledgements

The authors greatly acknowledge the experimental support of Christina Odemer and Holger Geßwein. This work has been carried out within the framework of the EUROfusion Consortium, funded by the European Union via the Euratom Research and Training Programme (Grant Agreement No 101052200 — EUROfusion). Views and opinions expressed are however those of the author(s) only and do not necessarily reflect those of the European Union or the European Commission. Neither the European Union nor the European Commission can be held responsible for them.

Appendix A. Supplementary data

Supplementary data to this article can be found online at https://doi.org/10.1016/j.nme.2024.101650.

References

[1] O. Leys, J.M. Leys, R. Knitter, Current status and future perspectives of EU ceramic breeder development, Fusion Eng. Des. 164 (2021) 112171, https://doi.org/10.1016/j.fusengdes.2020.112171.
[2] L.V. Boccaccini, F. Arbeiter, P. Arena, J. Aubert, L. Bühler, G. Zhou, Status of maturation of critical technologies and systems design: Breeding blanket, Fusion Eng. Des. 179 (2022) 113116, https://doi.org/10.1016/j.fusengdes.2022.113116.
[3] D.A.H. Hanaor, M.H.H. Kolb, Y. Gan, M. Kamlah, R. Knitter, Solution based synthesis of mixed-phase materials in the Li_2TiO_3–Li_4SiO_4 system, J. Nucl. Mater. 456 (2015) 151–161, https://doi.org/10.1016/j.jnucmat.2014.09.028.
[4] S. Claus, H. Kleykamp, W. Smykatz-Kloss, Phase equilibria in the Li_4SiO_4–Li_2SiO_3 region of the pseudobinary Li_2O–SiO_2 system, J. Nucl. Mater. 230 (1996) 8–11, https://doi.org/10.1016/0022-3115(96)00022-0.
[5] G. Izquierdo, A.R. West, Phase equilibria in the system Li_2O–TiO_2, Mater. Res. Bull. 15 (1980) 1655–1660, https://doi.org/10.1016/0025-5408(80)90248-2.
[6] J.A. Mergos, C.T. Dervos, Structural and dielectric properties of Li_2O-doped TiO_2, Mater. Charact. 60 (2009) 848–857, https://doi.org/10.1016/j.matchar.2009.01.019.
[7] J. Leys, R. Rolli, H.-C. Schneider, R. Knitter, HICU PIE results of neutron-irradiated lithium metatitanate pebbles, Nucl. Mater. Energy 38 (2024) 101625, https://doi.org/10.1016/j.nme.2024.101625.
[8] F.A. Hernández, G. Zhou, Current design of the EU DEMO Helium Cooled Pebble Bed breeding blanket, Proceedings of the 15th International Workshop on Beryllium Technology (BeWS-15) September, 14-15, 2022, Karlsruhe, Germany, KIT Sci. Rep. 7764 (2023) 70–78, https://doi.org/10.5445/IR/1000160101.
[9] M. Xiang, Y. Zhang, Y. Zhang, S. Liu, H. Liu, C. Wang, Fabrication and characterization of Li_2TiO_3–Li_4SiO_4 pebbles for tritium breeder, J. Fusion Energ. 34 (2015) 1341–1347, https://doi.org/10.1007/s10894-015-9967-7.
[10] H. Völlenkle, A. Wittmann, H. Nowotny, Die Kristallstruktur von Li_4SiO_4, Monatsh. Chem. 99 (1968) 1360–1371, https://doi.org/10.1007/BF00902680.
[11] H. Seemann, Die Kristallstruktur des Lithiummetasilikates, $(Li_2SiO_3)_x$, Acta Crystallogr. 9 (1956) 251–252, https://doi.org/10.1107/S0365110X56000693.
[12] J.F. Dorrian, R.E. Newnham, Refinement of the structure of Li_2TiO_3, Mater. Res. Bull. 4 (1969) 179–183, https://doi.org/10.1016/0025-5408(69)90054-3.
[13] Z. Liu, N. Zhang, K. Sun, A novel grain restraint strategy to synthesize highly crystallized $Li_4Ti_5O_{12}$ (~20 nm) for lithium ion batteries with superior high-rate performance, J. Mater. Chem. 22 (2012) 11688–11693, https://doi.org/10.1039/C2JM31066J.
[14] M. Asou, T. Terai, Y. Takahashi, High-temperature enthalpy-increment measurements and derived heat capacity of lithium orthosilicate (Li_4SiO_4) at temperatures from 300 K to 1000 K, J. Chem. Thermodyn. 24 (1992) 273–280, https://doi.org/10.1016/S0021-9614(05)80067-9.
[15] H. Kleykamp, Enthalpy, heat capacity, second-order transitions and enthalpy of fusion of Li_4SiO_4 by high-temperature calorimetry, Thermochim. Acta 287 (1996) 191–201, https://doi.org/10.1016/S0040-6031(96)02996-6.
[16] H. Kleykamp, Phase equilibria in the Li-Ti-O system and physical properties of Li_2TiO_3, Fusion Eng. Des. 61–62 (2002) 361–366, https://doi.org/10.1016/S0920-3796(02)00120-5.